Journal of Water Resource and Protection, 2022, 14, 433-455
https://www.scirp.org/journal/jwarp
ISSN Online: 1945-3108
ISSN Print: 1945-3094

Hydrogeochemistry of Shale-Limestone-Mudstone Successions Aquifers—The Case of the Hantebet Sub Basin in Northern Ethiopia

Nata T. Tafesse[1*], Bheemalingeswara Konka[2], Berhanu F. Alemaw[1]

[1]Geology Department, Faculty of Sciences, University of Botswana, Gaborone, Botswana
[2]Department of Mining and Geological Engineering, FET, Botswana International University of Science and Technology, Palapye, Botswana
Email: *tafessen@ub.ac.bw, Alemaw@ub.ac.bw, kbheema2006@gmail.com

How to cite this paper: Tafesse, N.T., Konka, B and Alemaw, B.F. (2022) Hydrogeochemistry of Shale-Limestone-Mudstone Successions Aquifers—The Case of the Hantebet Sub Basin in Northern Ethiopia. *Journal of Water Resource and Protection*, **14**, 433-455.
https://doi.org/10.4236/jwarp.2022.146023

Received: March 3, 2022
Accepted: June 19, 2022
Published: June 22, 2022

Abstract

The present paper provides evidence of the possible impact of shale-limestone-mudstone successions aquifers on groundwater chemistry by assessing the different hydrogeochemical processes. This was done by considering a sedimentary aquifer basin, namely the Hantebet sub basin (24.4 km^2), Tekeze basin, northern Ethiopia. Groundwater is the main source of water supply in the sub basin extracted using hand dug wells, for domestic, irrigation and livestock uses. The sub basin is dominated by Paleozoic-Mesozoic sedimentary successions. Twenty groundwater samples were collected from hand dug wells using depth-integrated sampling techniques from both confined and unconfined aquifers. The major water bearing formations are gravely sand, weathered shale and weathered and fractured limestone, and intercalated weathered and fractured limestone and mudstone. The results indicate that groundwater is acidic to neutral, fresh, and hard to very hard. Ca^{2+}, Na^{+}, HCO_3^{-} and SO_4^{2-} are dominant ions compared to Mg^{2+}, K^{+}, and Cl^{-} ions which show low to very low concentrations. Among eight hydrochemical facies identified, Ca-Na-HCO_3 (40%), Ca-HCO_3 (20%), Ca-Mg-Na-HCO_3 (10%) and Ca-Na-HCO_3-SO_4 (10%) types dominate water chemistry. Dissolution of calcite and gypsum, and hydrolysis of feldspars, plagioclase, biotite and pyroxene are the major geochemical processes that control the chemistry of groundwater in the area. The intercalated shale beds are the source of sodium and chloride ions. Since, this study is based on groundwater from hand dug wells, the conclusions of this study should be further verified using groundwater from deep wells that are drilled in these successions.

Keywords

Confined Aquifer, Dissolution, Ethiopia, Groundwater, Hydrolysis, Unconfined Aquifer

1. Introduction

1.1. Background

Groundwater is the world's largest accessible freshwater and an important resource for domestic water supply, irrigation, livestock's, and industrial uses as well as for global food security [1]. According to United Nations Environment Program report (UNEP) [2] approximately one-third of the world's population depends on groundwater for drinking purpose. Like in many countries, groundwater is the main source of water supply for domestic, irrigation, livestock's and industrial uses in both urban and rural areas of Ethiopia. Especially in the arid and semi-arid parts of the country it remains the sole source of water supply for different uses. Hand dug wells, boreholes and springs are developed and used to meet the demands. However, groundwater that serves as a source of water supply varies in its chemistry throughout the country depending on the geological, anthropogenic and other conditions.

Groundwater gets its chemical character from the rocks and sediments through which it percolates by different geochemical processes. However, there are many factors that determine the chemical composition of the groundwater. These include, initial composition of rain, degree of chemical weathering, geology of the area, overlying land uses, recharge sources, nearness to the seaside, aquifer type, aquifer depth, anthropogenic, time etc.

The study area, Hantebet sub basin, 24.4 km^2, forms part of Takeze basin, Tigray region, northern Ethiopia. It is located about 55 km south of the Mekelle city, capital of Tigray region, bounded by latitude 1,467,000 to 1,476,000 m N and longitude 523,000 to 530,000 m E (**Figure 1**). Groundwater is the main source of water supply for local domestic and irrigation uses. It is extracted using hand dug wells, more than 156 are found in different parts of the sub basin. Treadle pump and Afridev hand pumps (**Figure 2**) are used for abstraction of the groundwater. Treadle pump is a human-powered suction pump designed to lift water from a depth of seven meters or less. Unlike other types of pumps, it sits on top of the well. The pumping is activated by stepping up and down on a treadle, which are levers, which drive pistons, creating cylinder suction that draws groundwater to the surface. Afridev hand pump is a manually operated pump that uses human power to lift water from a depth of 10 to 45 m. It is a conventional lever action hand pump. Pulley system is also used by few farmers.

In the area of study topography varies significantly. Elevation ranges from

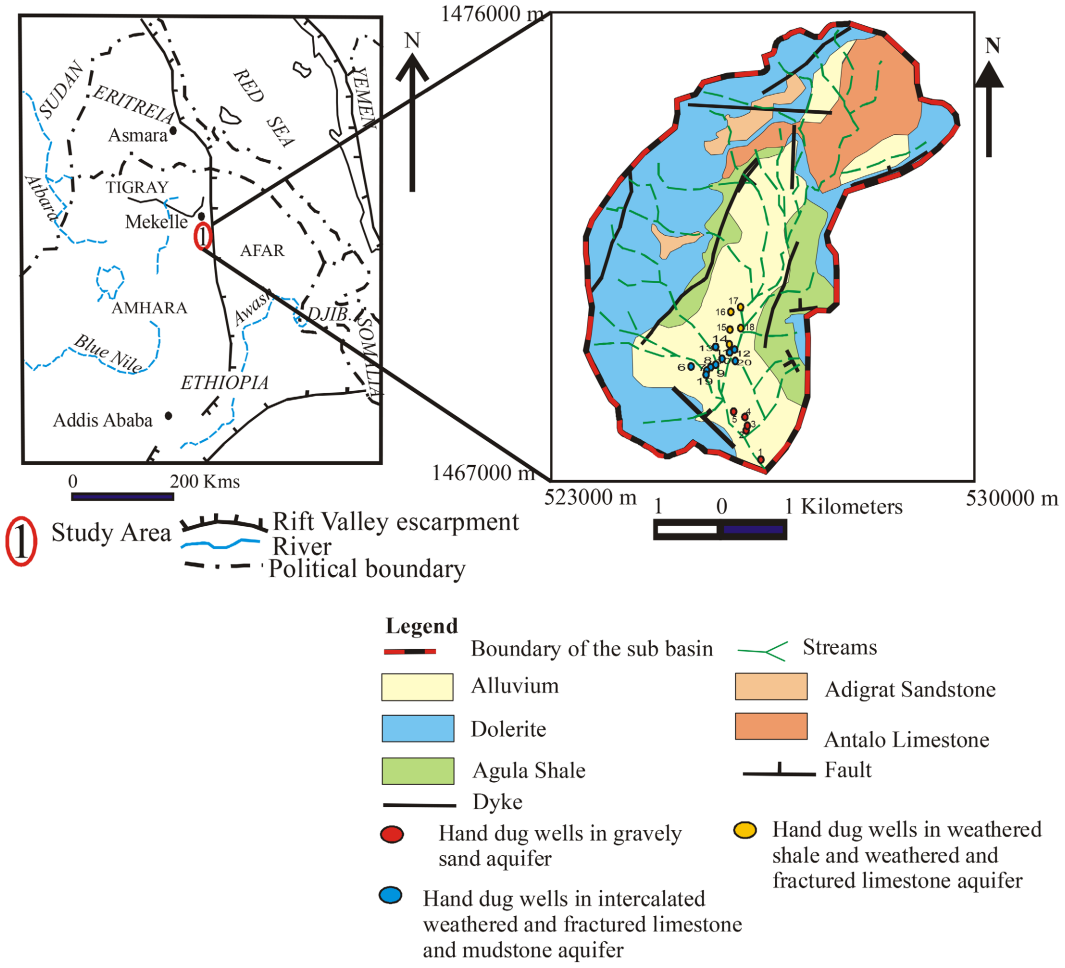

Figure 1. Location and geological map of the study area [3] [4] [5].

Figure 2. Groundwater abstraction in the study area [Treadle pump showing sticks used to support the persons who power the treadle pump during abstractions].

2000 m above sea level on the lowland to mountain peaks greater than 2600 m above sea level. The average elevation is 2330 m. The mean annual minimum and maximum air temperature in the area is 11.15˚C and 23.39˚C, respectively. The mean annual air temperature and rainfall is 17.3˚C and 632.08 mm [3], respectively. The area is drained by a perennial river called "Hantebet". It originates

from the northern highlands and flows towards the southern flatlands and finally joins the Tekeze River, which in turn is tributary of Atbarah River in Sudan.

The area is dominated by Paleozoic-Mesozoic sedimentary successions that form part of Mekelle basin (also referred as Mekelle Outlier). Few studies on the geology of Mekelle basin have been conducted recently [6] [7]. However, in the past the basin was widely studied by many researchers [8]-[17]. Even though such ample geological studies are found in the basin, only limited studies are there on the impact of Paleozoic-Mesozoic sedimentary successions on groundwater chemistry in different parts of the Basin [18] [19]. The present paper provides an evaluation of the impact of shale-limestone-mudstone successions aquifers on groundwater chemistry of the Hantebet sub basin. The specific objectives of the manuscript are: 1) identification of the different geological formations that serve as an aquifer; 2) determination of the types of aquifers in the sub-basin; and 3) determination of the hydrogeochemical processes that control the chemistry of groundwater.

1.2. Geology the Mekelle Basin

The Mekelle Basin having a semi-circular shape is covering about 8000 km^2. The stratigraphic succession of northern Ethiopia is divided based on age, genesis, and composition. They include (from oldest to the youngest): low-grade metamorphic rocks of Neoproterozoic age (forming the base), Enticho Sandstone Formation and Edaga Arbi Tillite Formation of Paleozoic age, Adigrat Sandstone Formation, Antalo Limestone Formation, Agula Shale Formation, and Amba Aradam Formation (of Mesozoic age), followed younger Cenozoic age Trap series, Mekelle Dolerites, and Axum-Adwa Plugs [8] [17]. The Neoproterozoic basement is the southern extension of Arabian-Nubian Shield (ANS) and the Paleozoic clastic sedimentary rocks are characteristic of northern Ethiopia. The Enticho Sandstone, about 200 m thick, rests unconformably on the basement [9]. The Sandstone is composed of white, coarse grained, cross-bedded, calcareous sandstone containing lenses of siltstone, grit and polymict conglomerate with subrounded to well-rounded pebbles, cobbles, and boulders. Scattered, mainly granite and gneiss are also common at places. It shows poorly sorting as it is an immature deposit. The Edaga Arbi Tillite vary in thickness from 150 to 180 m. They are formed by basal massive greywackes (~20 to 50 m thick) with a fine-grained matrix embedding clasts of gneiss, granite and metavolcanics, up to 6 m diameter, frequently striated; and by a variegated colored sequence, 130 m thick, of siltites followed by shales and argillites. The siltitic lower portion still contains clasts up to 50 cm, and the shaly upper portion contains harder calcareous and dolomitic thin beds. The siltites and shales with pebbles overlying the basal tillites seem to be belonging to the same sedimentary cycle as the tillites. The tillite overlies the Enticho Sandstone, however, the latter is reported to interfinger with the glacial rocks at several places far north outside the Mekelle basin between Adwa and Adigrat towns.

The Mesozoic sedimentary successions have Adigrat Sandstone Formation (at the base resting at places unconformably on basement Precambrian or thin Paleozoic rocks) followed by Antallo Limestone Formation, and Agula Shale Formation of Jurassic age, and Amba Aradam (or Upper Sandstone) Sandstone Formation of Cretaceous age. These are later intruded by younger dolerite dykes/sills (referred as Mekelle dolerite) during Oligocene (31 - 26 Ma). The Mesozoic sedimentary successions, about 3 km thick, are produced by marine transgression and regression.

Adigrat sandstone is red to pink in color, fine to medium grained, well-sorted, ferruginous, and dominated by sand size quartz. It is non-calcareous except at the top near the contact with the overlying Antalo limestone, where thin beds of limestone have developed. It shows deep vertical joints, cross bedding, with thin bands of ferruginous mud (<1 m), and at places development of laterite about 2 m thick. Thickness of the sandstone increase from north to south with maximum thickness of about 600 m aligned in a NNE–SSW direction, west of Mekelle Basin [8].

According to Andrea *et al.* [8] Antalo Limestone consists of four facies (from bottom to top), 1) a sandy oolite limestones with low amount of marls, few chert beds and a fauna of corals, gastropods, and echinoids; 2) an interbedding of marls and limestones with brachiopods and algal and chert beds; 3) reef limestones interbedded with marls and stromatolites; and, 4) black to grey microcrystalline limestones interbedded with marls [11]. In the northern Ethiopia, the thickness of the Antalo Limestone ranges from 300 m to 800 m. The Agula Shale overlies the Antalo limestone and shows gray-green and black color, interlaminated with marl and claystone, with finely crystalline black limestone containing disseminated pyrite with some gastropods and brachiopods. It also contains some thin beds of gypsum and dolomite and a few beds of yellow coquina and reaches a maximum thickness of 300 m [15].

According Beyth [10], Amba Aradam Sandstone is identified by two main facies: 1) white to pink in colour, intercalated with clay and silt bands, interbedded with medium- to coarse grained quartz, exposed in north-western part of Mekelle Basin. Upper part contains tuffaceous mudstone and lateritized; 2) white in colour, with clayey beds and exposed in the southern part of the Basin. The Amba Aradam Sandstone has a maximum thickness of 200 m and lies unconformably on the Agula Shales [11]. Flood basalts represent Trap series, unconformably overlie the sedimentary successions. Flood basalts are black in colour, phenocrysts of olivine are common (olivine basalt), shows coarse sub-ophitic to intergranular texture. It is characterized by numerous flows with well-developed columnar jointing, at places shows development of zeolites as amygdaloids and paleosols. Interbedded lacustrine deposits of off-white silicified limestone, and diatomite with gastropods occur at several levels [10].

Numerous dolerite dykes and sills, with black colour and ophitic texture occur in Mekelle Basin. They intrude the sedimentary and basement rocks in the Basin. They are comagmatic with the Trap Series volcanics [20], some of them being

feeders for eruptions of the Trap Series. Most of them strike northwest or north-northwest and are parallel to the Red Sea-Afar Escarpment trend.

1.3. Geology of the Study Area

The study area consists of Adigrat sandstone, Antalo limestone, Agula shale and intrusive rocks. Alluvial sediments present in the low-lying areas and cover the rock units (**Figure 1**).

Shale

It shows intercalations at places with limestone, exposed in the east, southeast, central-west and north-western parts of the study area and cover about 13.4% of the study area. It is also exposed in the lowlands along the river beds and is covered by thick alluvial sediments. It shows variegated colors, light brown/green color at the bottom, red color in the middle and olive color on the top. It is highly weathered and fractured. Weathered portions of the rock shows dark grey color. According to Nata *et al.* [21], it is dominated by clay, followed by fine grained mica and quartz. Rocks gently dip towards east and is characterized by primary and secondary structures.

Limestone

It covers about 12% of the total study area and exposed in the northern and north-eastern parts of the study area having an average exposed thickness of 8 m. The rock is composed of calcite (80% to 56%), quartz (6% to 2%), opaque (Fe-oxide) (~3%), feldspar (2% to 1%), gypsum (~2%), and sphene (1% to nil). Its fossil content ranges from trace to 32% [21].

Sandstone

It shows predominantly red colour, at places shows white colour, cross bedded, ripple marked, hard, and medium to fine grained rock exposed in the north-western and western parts covering about 0.5% of the total study area with an average exposed thickness of 10 m. The rock is composed of quartz (57% to 55%), feldspar (15%), biotite (10% to 5%), opaque (Fe–oxide) (6% to 3%), epidote (17% to 1%), sphene (~10%), and plagioclase (~6%) [21]. Fractures with different orientations are present and is highly altered along contact with intrusive. At places, along the river-beds and gully exposures, sandstone shows calcareous nature. Also shows systematically developed joints which are widened later due to solution activity. The open spaces range in width from 14 to 30 cm.

Dolerite

These younger intrusive bodies occur as sills and dykes and are characterized by a moderate to highly weathered (spheroidal/ onion shape) surface with yellowish-brown color, covering about 45.2% of the total study area almost encircled the whole area. The sills are found forming steep cliffs and/or flat mountain tops. Fresh dolerites are dark, medium grained and highly fractured rocks. The fractures are oriented in both NW and SW directions. The rocks are composed of plagioclase (46% to 40%), pyroxene (37% to 32%), opaque (Fe-oxide) (10% to 8%), biotite (8% to 2%), apatite (~10%) and olivine (~7%) [21].

Alluvial Deposit

These are recent Quaternary deposits found in the valley between the ridges and cover about 28.9% of the total study area. They are overlying the Paleozoic-Mesozoic sedimentary successions of the sub basin, and are composed of very fine to coarse grained material, ranging from clay to sand to boulder size materials. The boulders are dominant around the mouth of the catchments or recharge area, dominated by the fragments of dolerites with an average size of 50 cm and followed by limestone to sandstone. The shapes of the fragments vary from angular to sub-angular to rounded. The average thickness of these deposits is ~6 m.

2. Methodology

2.1. Samples Collection

Twenty groundwater samples were collected from open hand dug wells that were drilled in different aquifers from various locations (**Figure 1**). Prior to sampling, the hand dug wells selected for the study were purged for about six to ten minutes to ensure that the standing water did not contaminate the sample and the groundwater that was taken was from the aquifer. All the samples were taken at low water levels. Each sample was filtered and collected in 500 ml plastic bottle, and the sampling bottle was rinsed repeatedly with distilled water before taking the samples. After sampling the bottles were tightly covered with caps and sealed with tap to minimize oxygen contamination and the escape of dissolved gases. At each sample station two water samples were taken. One is acidified with a drop of nitric acid and another without acidification. The samples were kept in cold place to minimize chance of chemical reaction which can result in precipitation of dissolved elements. At each site the information related to depth to the groundwater, lithology and water-bearing formations were recorded. Physico-chemical parameters such as pH, temperature, electrical conductivity (EC) and total dissolved solids (TDS) were measured in situ using multi-parameter probe model Hanna. The samples were again tested for these physico-chemical parameters in the laboratory to cross check the data.

2.2. Sample Analyses

The groundwater samples were analyzed in the Water Works Design and Supervision Enterprise Laboratory Service, Addis Ababa. Elements Na, K, Ca, and Mg were analyzed using Atomic Absorption Spectrophotometer (AAS) while Cl^-, SO_4^{2-} and NO_3^- ions were analyzed using ion chromatograph. HCO_3^- and CO_3^{2-} ions were analyzed and using titration method. Computation of electro neutrality was done using Equation (1) to check the accuracy of the analyses. In the equation, the cations and anions are expressed as meq/l. The sums of cations (Ca^{2+}, Mg^{2+}, K^+, and Na^+), and anions (HCO_3^-, Cl^-, SO_4^{2-} and NO_3^-) were used. The computed values range from 0.44 to 2.17, which is in the acceptable range.

$$\text{Electro neutrality}\left(\text{E.N}\right)=\left[\frac{\text{Sum of Cations}-\text{Sum of Anions}}{\text{Sum of Cations}+\text{Sum of Anions}}\right]\times 100 \quad (1)$$

The saturation index (SI) is calculated for all the analyzed samples for calcite using Aquachem software. SI is determined using Equation (2), which is the logarithm of the ratio of the ion activity product (IAP) of a solute to its solubility product (Ksp) at a given temperature [22]. Accordingly, if SI < 0, SI = 0, and SI > 0, the water is undersaturated, equilibrium, and oversaturated conditions, respectively [23].

$$\text{SI}=\log_{10}\frac{\text{IAP}}{\text{Ksp}} \quad (2)$$

2.3. Data Processing

Aquachem 4.0 software, a fully integrated statistical package developed specifically for graphical and numerical analyses of aqueous geochemical data sets, was used to process the chemical data. Simple descriptive statistical methods, ionic ratio analyses, computations of chloro-alkaline indices (CAI 1 and CAI 2), bivariate plots and regression analyses were used to treat the data. Computations of chloro-alkaline indices (CAI 1 and CAI 2) were done using the Equations (3) and (4) [24] [25]:

$$\text{CAI 1}=\frac{\text{Cl}-\left(\text{Na}-\text{K}\right)}{\text{Cl}} \quad (3)$$

$$\text{CAI 2}=\frac{\text{Cl}-\left(\text{Na}-\text{K}\right)}{\text{SO}_4+\text{HCO}_3+\text{NO}_3+\text{CO}_3} \quad (4)$$

Location and geological map of the study area together with the location of hand dug well sites was produced by using ArcView 3.3 and CorelDRAW 12 software's.

3. Results

Hydrogeochemistry

pH values of groundwater ranges from 6.55 to 7.26 and predominantly (85%) acidic in character (**Table 1**). Electrical conductivity (EC) values range from 600 - 1120 μS/cm with a mean of 817 μS/cm and shows inverse relation with pH (**Figure 3(a)**). TDS values range from 300 - 570 mg/l with a mean of 393.5 mg/l. Both EC and TDS show similar trend and indicate that higher the pH lower is the content of elements in the sample (**Figure 3(b)** & **Figure 3(c)**).

Water hardness values calculated based on Ca and Mg range from 241.5 to 430.5 mg/l $CaCO_3$ with an average concentration of 306.915 mg/l $CaCO_3$. Alkalinity values range from 256.2 to 483 mg/l $CaCO_3$ with an average concentration of 344.610 mg/l $CaCO_3$. The trends of both hardness and alkalinity are shown in **Figure 4**.

The description of the variables in **Table 1** are EC (μS/cm at 25˚C) is electrical conductivity: TDS (mg/l) is total dissolved solids: HD is hardness in mg/l $CaCO_3$:

Alk is alkalinity in mg/l $CaCO_3$: IWFLM is intercalated weathered and fractured limestone and mudstone: WSWFL: weathered shale and weathered and fractured limestone: and, GNA is geological nature of the aquifer.

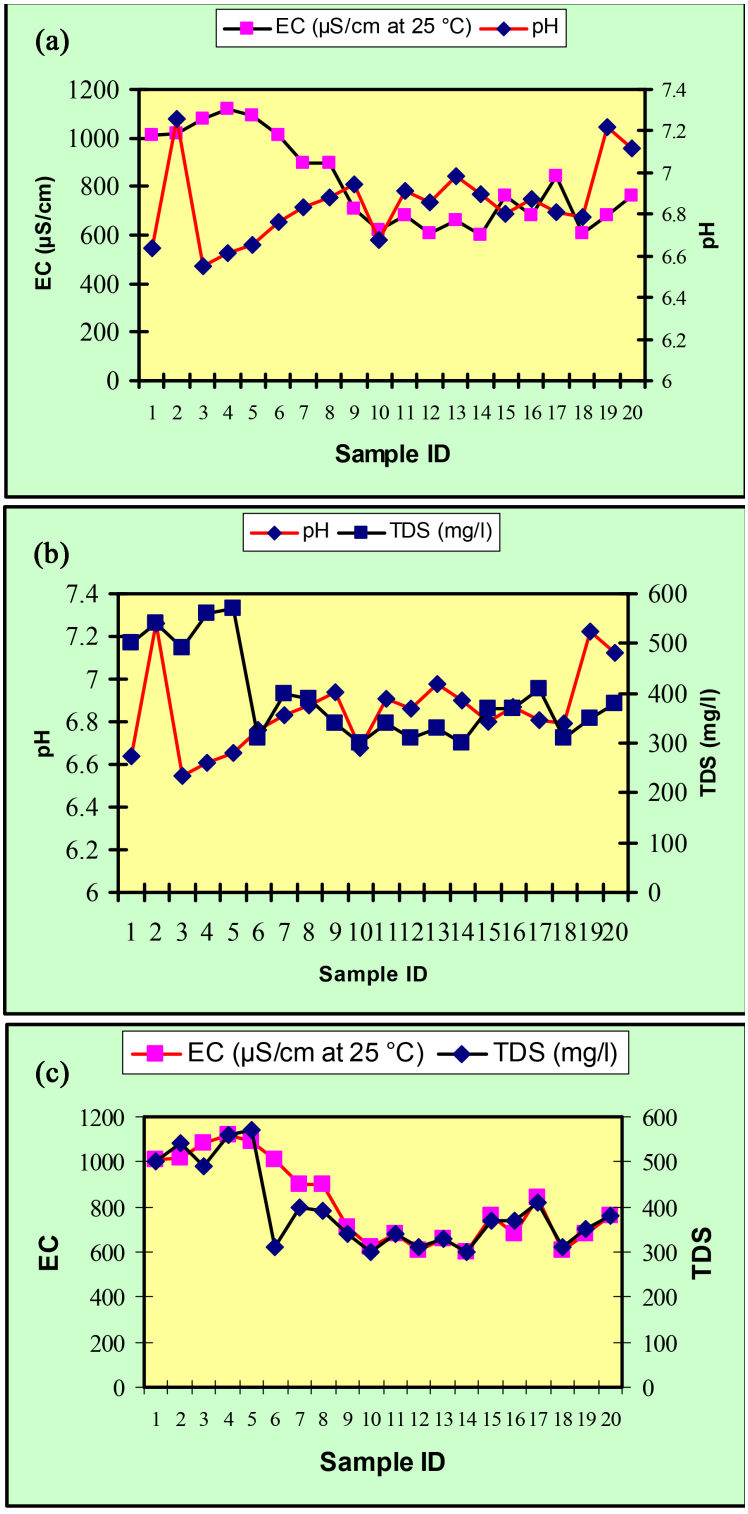

Figure 3. (a) Electrical conductivity (µS/cm) and pH; (b) TDS (mg/l) and pH; (c) Electrical conductivity (µS/cm) and TDS (mg/l) of the groundwater, Hantebet sub basin.

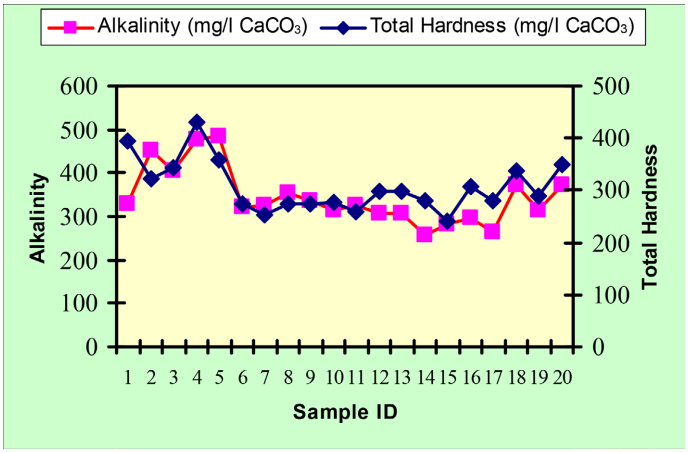

Figure 4. Alkalinity and hardness (mg/l $CaCO_3$) of the groundwater, Hantebet sub basin.

Table 1. Summarized results of the physico-chemical parameters of the analyzed groundwater samples, Hantebet sub basin.

No.	Sample Code	EC	TDS	pH	HD	Alk	Water Type	GNA
1	HAGW-S1	1010	500	6.64	394.8	327.6	Ca-Mg-HCO_3-SO_4	Gravely sand
2	HAGW-S2	1020	540	7.26	323.4	451.5	Na-Ca-HCO_3-SO_4	Gravely sand
3	HAGW-S3	1080	490	6.55	342.3	403.2	Ca-Mg-Na-HCO_3	Gravely sand
4	HAGW-S4	1120	560	6.61	430.5	476.7	Ca-Na-Mg-HCO_3	Gravely sand
5	HAGW-S5	1090	570	6.65	357	483	Ca-Mg-Na-HCO_3	Gravely sand
6	HAGW-S6	1010	310	6.76	275.1	321.3	Ca-HCO_3	IWFLM
7	HAGW-S7	900	400	6.83	254.1	325.5	Ca-Na-HCO_3	IWFLM
8	HAGW-S8	900	390	6.88	273	352.8	Ca-Na-HCO_3	IWFLM
9	HAGW-S9	710	340	6.94	273	336	Ca-Na-HCO_3	IWFLM
10	HAGW-S10	620	300	6.68	277.2	315	Ca-Na-Mg-HCO_3-SO_4	IWFLM
11	HAGW-S11	680	340	6.91	258.3	325.5	Ca-Na-HCO_3	IWFLM
12	HAGW-S12	610	310	6.86	298.2	308.7	Ca-Na-HCO_3	IWFLM
13	HAGW-S13	660	330	6.98	298.2	308.7	Ca-Na-HCO_3	IWFLM
14	HAGW-S14	600	300	6.90	279.3	256.2	Ca-Na-HCO_3-SO_4	WSWFL
15	HAGW-S15	760	370	6.80	241.5	283.5	Ca-Na-HCO_3-SO_4	WSWFL
16	HAGW-S16	680	370	6.87	308.7	296.1	Ca-HCO_3	WSWFL
17	HAGW-S17	840	410	6.81	281.4	262.5	Ca-HCO_3	WSWFL
18	HAGW-S18	610	310	6.79	336	371.7	Ca-Na-HCO_3	WSWFL
19	HAGW-S19	680	350	7.22	287.7	312.9	Ca-HCO_3	IWFLM
20	HAGW-S20	760	380	7.12	348.6	373.8	Ca-Na-HCO_3	IWFLM

The chemical analysis results of the groundwater samples plotted in Piper diagram, yielded the following water types (Table 2, Figure 5). 40% of samples are Ca-Na-HCO_3 type, 20% Ca-HCO_3 type, and 10% Ca-Na-HCO_3-SO_4 type. The remaining types Ca-Mg-HCO_3-SO_4, Na-Ca-HCO_3-SO_4, Ca-Mg-Na-HCO_3,

Ca-Na-Mg-HCO_3, Ca-Mg-Na-HCO_3 and Ca-Na-Mg-HCO_3-SO_4 account 5% each. Groundwater is dominated by calcium ion among others (Figure 5 and Figure 6, and Table 2), having concentrations ranging from 75.6 to 117.60 mg/l with an average concentration of 94.236 mg/l. Magnesium shows similar trend like Ca ranging from 4.59 to 33.15 mg/l with an average concentration of 17.339 mg/l. The concentrations of sodium range from 22.5 to 128 mg/l with an average concentration of 50.275 mg/l. Concentrations of potassium range from 0.2 to 5.3 mg/l with an average concentration of 0.975 mg/l. Generally, based on the mean values of the chemical parameters, the cations were in the order of abundance as

Table 2. Summarized results of the analyzed groundwater samples (in mg/l), Hantebet sub basin.

No.	Sample Code	Na^+	K^+	Ca^{2+}	Mg^{2+}	Cl^-	SO_4^{2-}	NO_3^-	HCO_3^-
1	HAGW-S1	33	1.7	114.24	26.5	19.57	148	2.1	399.67
2	HAGW-S2	128	0.6	84.84	27.03	46.35	136	0.97	550.83
3	HAGW-S3	47	0.7	93.84	26.52	25.75	47.6	2.09	491.9
4	HAGW-S4	68	5.3	117.6	33.15	49.44	88.6	0.4	581.57
5	HAGW-S5	58	0.7	88.2	33.15	22.66	16.3	0.4	589.26
6	HAGW-S6	29	2	96.6	8.16	17.5	23.6	0.49	391.98
7	HAGW-S7	61	0.5	79.8	13.26	21.63	65.2	0.64	397.11
8	HAGW-S8	51	0.3	84	15.3	15.45	43.6	0.5	430.42
9	HAGW-S9	48	0.5	84.84	14.79	18.54	44.8	0.55	409.92
10	HAGW-S10	56	0.4	75.6	21.42	23.69	80.3	0.75	384.3
11	HAGW-S11	49	0.5	94.08	5.61	22.66	39.39	0.79	397.11
12	HAGW-S12	38	0.8	93.24	15.81	15.45	64.07	1.7	376.61
13	HAGW-S13	38	0.8	93.24	15.81	15.45	32.46	1.51	376.61
14	HAGW-S14	54	1	79.8	19.38	37.08	90.73	1.23	312.56
15	HAGW-S15	60	0.7	85.68	6.63	26.78	83.29	2.61	345.87
16	HAGW-S16	30	0.4	115.92	4.59	17.51	70.07	4.3	361.24
17	HAGW-S17	22.5	0.9	93.24	11.73	17.51	39.13	0.3	320.25
18	HAGW-S18	56	0.4	105.84	17.34	29.7	80.3	5.87	453.47
19	HAGW-S19	35	0.2	94.92	12.24	18.54	54.62	0.88	381.74
20	HAGW-S20	44	1.1	109.2	18.36	15.45	76.25	0.34	456.04
	Minimum	22.5	0.2	75.6	4.59	15.45	16.3	0.3	312.56
	Maximum	128	5.3	117.6	33.15	49.44	148	5.87	589.26
	Average	50.275	0.975	94.236	17.339	23.836	66.216	1.421	420.423
Standard Deviation		22.040	1.111	12.437	8.499	9.915	33.889	1.441	79.093

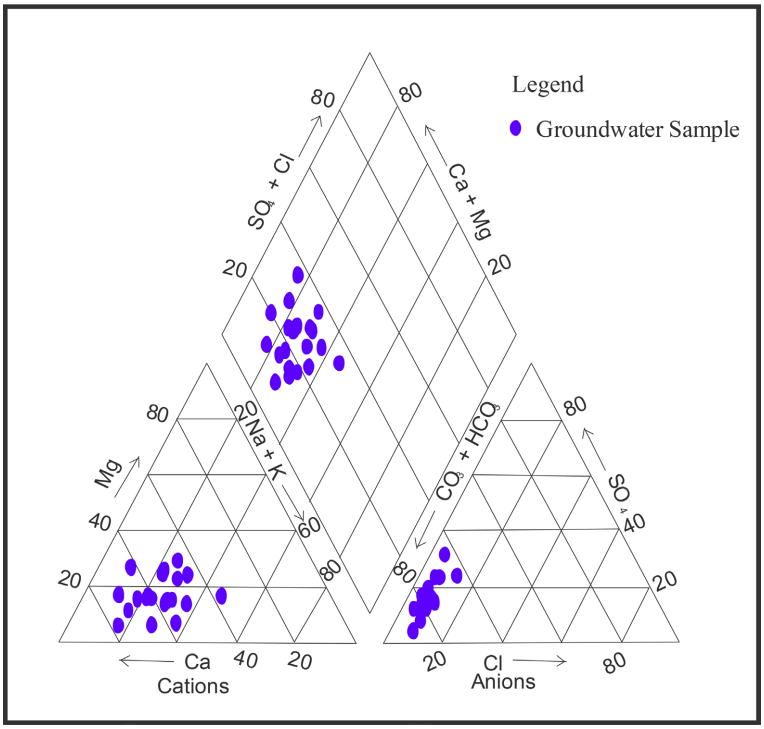

Figure 5. Piper diagram of the analyzed groundwater samples, Hantebet sub basin.

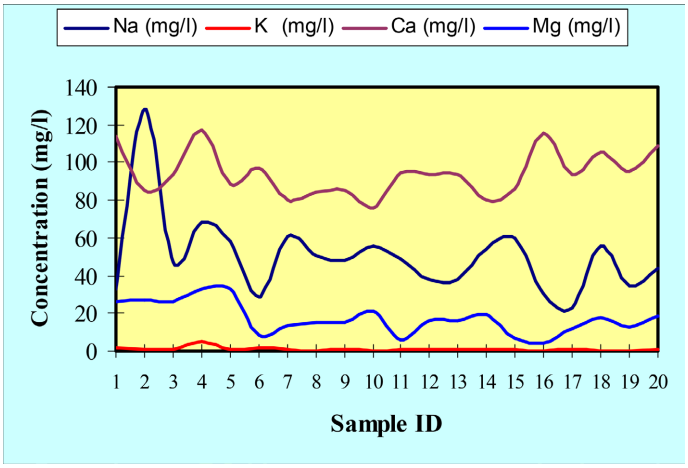

Figure 6. Major cations: Na^{+}, K^{+}, Ca^{+2} and Mg^{+2} in groundwater, Hantebet sub basin.

$Ca^{2+} > Na^{+} > Mg^{2+} > K^{+}$.

HCO_3^- ion concentrations range from 312.56 to 589.26 mg/l with average concentration of 420.423 mg/l (**Figure 5** and **Figure 7**, and **Table 2**). Carbonate values on the other hand are below detection levels in all the analyzed samples. Chloride values are much less in all the analyzed samples ranging from 15.45 to 49.44 mg/l with an average concentration of 23.836 mg/l. With the exception of hand dug well HAGW-S5, sulphate values are higher than chloride, and are ranging in values from 16.3 to 148 mg/l with an average concentration of 66.216 mg/l. Nitrate values range from 0.3 to 5.87 mg/l with an average concentration of 1.421 mg/l. Generally, based on the mean values of the chemical parameters,

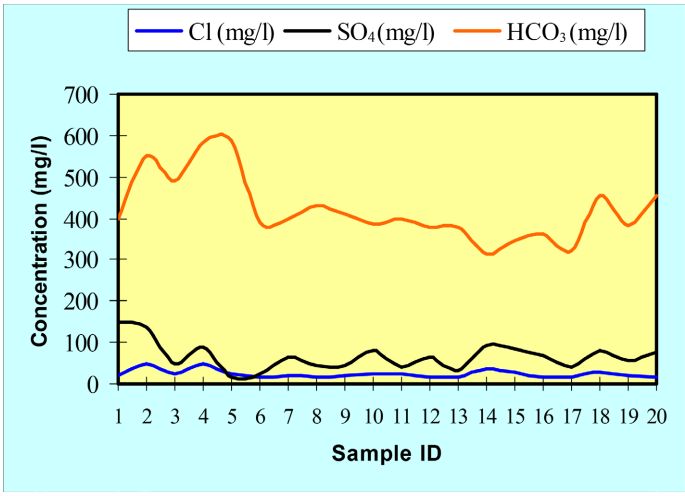

Figure 7. Major anions: Cl^-, SO_4^{2-}, and HCO_3^- in the analyzed groundwater, Hantebet sub basin.

the anions were in the order of abundance as $HCO_3^- > SO_4^{2-} > Cl^- > NO_3^-$.

Based on Soltan [26] and International Institute for Environment and Development (IIED) [27] classification of water, a classification based on milliequivalent per liter (meq/L), 65% of the analyzed groundwater is normal HCO_3^- type and the remaining 35% are normal SO_4^{2-} and Cl^- types (**Table 3**). According to Sakram and Adimalla [28], the classification scheme of Soltan [26] and IIED [27] is based on the respective concentration of HCO_3^-, SO_4^{2-} and Cl^- ions in the water: normal bicarbonate type if the bicarbonate ion concentrations varies between 2 and 7 meq/L, normal sulphate type if sulphate ion concentration is less than 6 meq/L and normal chlorine type if the concentration of chloride ion is less than 15 meq/L. This calcification is also revealed that weak acid surpass strong acids in the groundwater of the area.

The saturation index (SI) for calcite is given in **Table 3**. 75% of the samples have a saturation index zero and greater than zero whereas the remaining 25% have below zero. The samples that are undersaturated with respect to calcite are two samples from intercalated weathered and fractured limestone and mudstone aquifer and three samples from weathered shale and weathered and fractured limestone aquifer. Three samples from gravely sand aquifer, one from intercalated weathered and fractured limestone and mudstone aquifer and weathered shale and weathered and fractured limestone aquifer, respectively, are oversaturated with respect to calcite. Seven groundwater samples from intercalated weathered and fractured limestone and mudstone aquifer, two samples from gravely sand aquifer and one sample from weathered shale and weathered and fractured limestone aquifer are saturated with calcite.

4. Discussion

The hand dug wells sampled are ranging in depth from 1.3 to 10 m. These wells are penetrating only the upper most aquifers both unconfined and confined.

Table 3. Concentrations (in meq/L) of HCO_3^-, SO_4^{2-} and Cl^- ions and computed saturation index (SI) values of the analyzed groundwater samples, Hantebet sub-basin.

No.	Sample Code	Cl^-	SO_4^{2-}	HCO_3^-	Saturation Index (SI Calcite)
1	HAGW-S1	0.55	3.08	6.55	0.0
2	HAGW-S2	1.31	2.83	9.03	0.0
3	HAGW-S3	0.73	0.99	8.06	0.1
4	HAGW-S4	1.39	1.85	9.53	0.2
5	HAGW-S5	0.64	0.34	9.66	0.1
6	HAGW-S6	0.48	0.49	6.42	0.0
7	HAGW-S7	0.61	1.36	6.51	-0.1
8	HAGW-S8	0.44	0.91	7.05	0.0
9	HAGW-S9	0.52	0.93	6.72	0.0
10	HAGW-S10	0.67	1.67	6.30	-0.1
11	HAGW-S11	0.64	0.82	6.51	0.0
12	HAGW-S12	0.44	1.33	6.17	0.0
13	HAGW-S13	0.44	0.68	6.17	0.0
14	HAGW-S14	1.05	1.89	5.12	-0.2
15	HAGW-S15	0.76	1.74	5.67	-0.1
16	HAGW-S16	0.49	1.46	5.92	0.0
17	HAGW-S17	0.49	0.82	5.25	-0.1
18	HAGW-S18	0.84	1.67	7.43	0.1
19	HAGW-S19	0.52	1.14	6.26	0.0
20	HAGW-S20	0.44	1.59	7.47	0.1

These aquifers are formed by three different geological formations (Table 1): gravely sand, weathered shale and weathered and fractured limestone, and intercalated weathered and fractured limestone and mudstone. The impact of these different formations on the chemistry of the groundwater and the geochemical processes responsible for this are discussed as follows.

4.1. Intercalated Weathered and Fractured Limestone and Mudstone Aquifer

Three hydrochemical facies were identified in ten groundwater samples in the aquifer constituted by intercalated weathered and fractured limestone and mudstone. They include Ca-Na-HCO_3 (70%), Ca-HCO_3 (20%) and Ca-Na-Mg-HCO_3-SO_4 (10%). The groundwater is acidic to slightly neutral, fresh, and hard to very hard. The hardness is carbonate hardness. The alkalinity is ranging from 308.7 to 373.8 mg/l $CaCO_3$. In this groundwater Ca^{2+} is the dominant cation, followed by sodium (Na^+), magnesium (Mg^{2+}) and potassium (K^+) ions. HCO_3^- is the do-

minant anion and SO_4^{2-} is the second most abundant anion followed by Cl^-. Nitrate occurs in minor concentrations.

4.2. Weathered Shale and Weathered and Fractured Limestone Aquifer

Five groundwater samples were analyzed from this aquifer suggest that groundwater is slightly acidic, fresh (TDS less than 500 mg/l), and hard to very hard. The hardness is dominantly non-carbonate. Alkalinity of the groundwater ranges from 256.2 mg/l $CaCO_3$ to 371.7 mg/l $CaCO_3$. Three hydrochemical facies were identified in this aquifer, Ca-Na-HCO_3 (20%), Ca-HCO_3 (40%) and Ca-Na-HCO_3-SO_4 (40%). The water has a higher amount of alkaline earths (Ca^{2+} and Mg^{2+}) and a lower amount of alkalis (Na^+ and K^+). Without exception, Ca^{2+} is dominant over Mg^{2+}. There is a dominance of Na^+ over K^+, as sodium is more soluble than potassium, and the latter is more easily fixed on clay minerals in the rock matrix. K^+ is generally the least abundant of the cations. Among the anions, HCO_3^- is dominant over SO_4^{2-} and Cl^-. The anion Cl^- occurs in only minor concentrations whereas the concentration of SO_4^{2-} is significant.

4.3. Gravely Sand Aquifer

Five groundwater samples were analyzed from this aquifer and four hydrochemical facies were identified; Ca-Mg-Na-HCO_3 (40%), Ca-Na-Mg-HCO_3 (20%), Na-Ca-HCO_3-SO_4 (20%) and Ca-Mg-HCO_3-SO_4 (20%). The groundwater is acidic to neutral, fresh and hard to very hard. The hardness is carbonate hardness. The alkalinity ranges from 327.6 mg/l $CaCO_3$ to 483 mg/l $CaCO_3$. In this groundwater, except for one sample (Sample 2), in all the remaining samples Ca^{2+} is the dominant cation, followed by sodium (Na^+), magnesium (Mg^{2+}) and potassium (K^+) ions. In sample 2, Na^+ ion occurs as a dominant cation than Ca^{2+}. As shown in **Figure 6**, the difference in the concentration of Na ion between samples HAGW-S1 and HAGW–S2 is very high which is an indicative anomaly that further study is required to diagnose such variation within the same aquifer. Without exception HCO_3^- is the dominant anion and SO_4^{2-} is the second most abundant anion followed by Cl^- ion. The anion Cl^- occurs in only minor concentrations. Nitrate concentrations are insignificant.

4.4. Geochemical Processes

The computed Na/Cl and Na/Na + Cl ratios (**Table 4**) of the analyzed groundwater samples range from 2.00 - 5.05 and 0.67 - 0.83 with a mean of 3.32 and 0.76, respectively. These Na/Cl and Na/Na + Cl ratio values suggest that sodium ion has a source different from chloride-rich minerals such as halite, which can serve as a common source for both Na and Cl ions, and existence of some other process than dissolution of halite that release Na ion to groundwater having different geological nature. According to Sajil Kumar and James [29]; Meybeck [30]; Deutsch [31]; and Elango and Kannan [32], a molar ratio of Na/Cl greater than 1 indicates silicate weathering as a source of Na ion to the groundwater

chemistry. According to Adomako *et al.* [33], a molar ratio of Na/Na + Cl greater than 0.6 reflects Na ion released to groundwater by ion exchange process besides to silicate weathering.

As shown in **Table 4**, both CAI1 and CAI2 are negatives reflect Na and K ions are released due to normal ion exchange process: an exchange Ca and Mg ions in groundwater with K and Na ions in the sediments and rocks. The plot of $Ca^{2+} + Mg^{2+}$ versus $HCO_3^- + SO_4^{2-}$ (**Figure 8(a)**) where all the groundwater samples fall below the 1:1 line indicate both silicate weathering and ion exchange processes as the dominant processes [34] [35] [36] that control the chemistry of groundwater in the study area. However, the plot $(Ca^{2+} + Mg^{2+})$ - $(HCO_3^- - SO_4^{2-})$ versus Na^+-Cl^- (**Figure 8(b)**), most of the groundwater samples fall above the fitted regression line that has a slope of −0.498 and r^2 value of 0.08, suggesting that the respective groundwater samples are not mainly involved in normal ion exchange process and this process is not a prominent source for sodium and potassium ions to the groundwater. The dominancy of silicate weathering is further

Table 4. Calculated ionic ratios and Chloro-alkaline indices (CAI 1 and CAI 2) values of the analyzed groundwater samples, Hantebet sub basin.

No.	Sample Code	Na/Cl	Na/Na + Cl	CAI 1	CAI 2	Ca/Mg	$HCO_3^- / HCO_3^- + SO_4^{2-}$
1	HAGW-S1	2.62	0.72	−1.69	−0.10	2.61	0.68
2	HAGW-S2	4.25	0.81	−3.27	−0.36	1.91	0.76
3	HAGW-S3	2.79	0.74	−1.82	−0.15	2.15	0.89
4	HAGW-S4	2.13	0.68	−1.23	−0.15	2.15	0.84
5	HAGW-S5	3.94	0.80	−2.97	−0.19	1.61	0.97
6	HAGW-S6	2.35	0.70	−1.46	−0.10	7.19	0.93
7	HAGW-S7	4.34	0.81	−3.36	−0.26	3.65	0.83
8	HAGW-S8	5.05	0.83	−4.07	−0.22	3.33	0.89
9	HAGW-S9	4.02	0.80	−3.04	−0.21	3.47	0.88
10	HAGW-S10	3.64	0.78	−2.66	−0.22	2.14	0.79
11	HAGW-S11	3.33	0.77	−2.34	−0.20	10.20	0.89
12	HAGW-S12	3.75	0.79	−2.80	−0.16	3.58	0.82
13	HAGW-S13	3.75	0.79	−2.80	−0.18	3.58	0.90
14	HAGW-S14	2.24	0.69	−1.27	−0.19	2.50	0.73
15	HAGW-S15	3.43	0.77	−2.46	−0.25	7.78	0.77
16	HAGW-S16	2.65	0.73	−1.67	−0.11	15.21	0.80
17	HAGW-S17	2	0.67	−1.04	−0.08	4.79	0.86
18	HAGW-S18	2.90	0.74	−1.92	−0.18	3.69	0.82
19	HAGW-S19	2.92	0.75	−1.94	−0.14	4.69	0.85
20	HAGW-S20	4.34	0.81	−3.41	−0.17	3.61	0.82

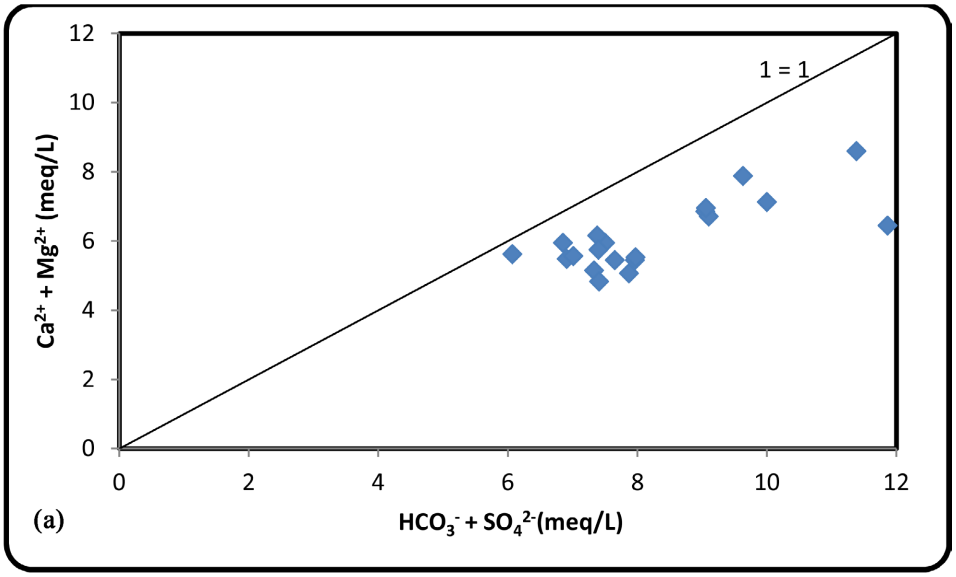
1 = 1
$Ca^{2+} + Mg^{2+}$ (meq/L)
$HCO_3^- + SO_4^{2-}$(meq/L)
(a)

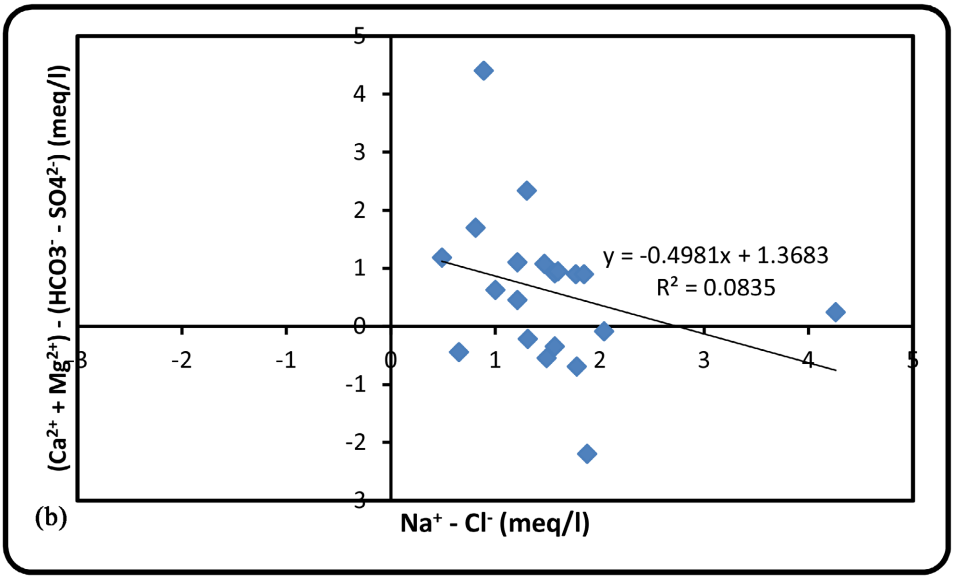
y = -0.4981x + 1.3683
R^2 = 0.0835
$(Ca^{2+} + Mg^{2+}) - (HCO3^- - SO4^{2-})$ (meq/l)
$Na^+ - Cl^-$ (meq/l)
(b)

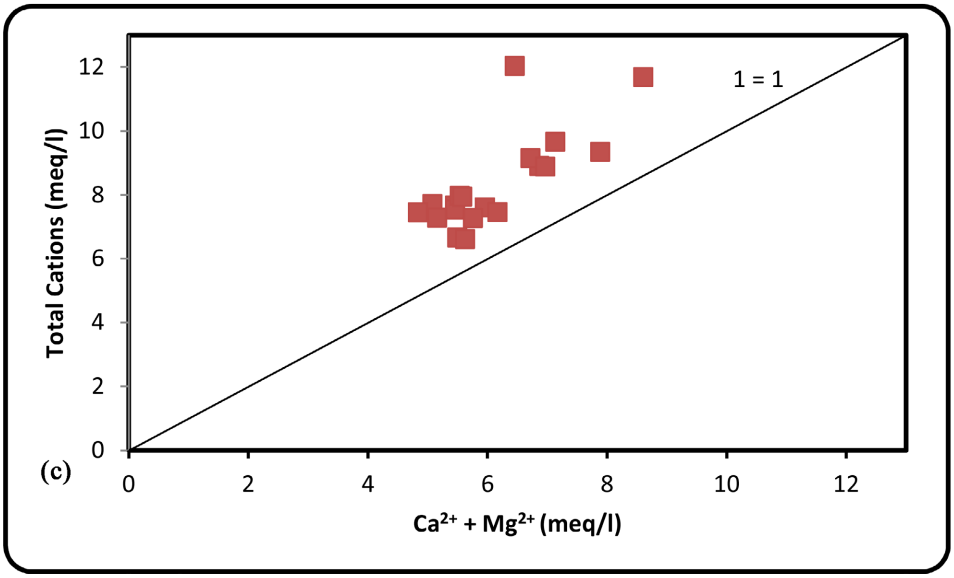
1 = 1
Total Cations (meq/l)
$Ca^{2+} + Mg^{2+}$ (meq/l)
(c)

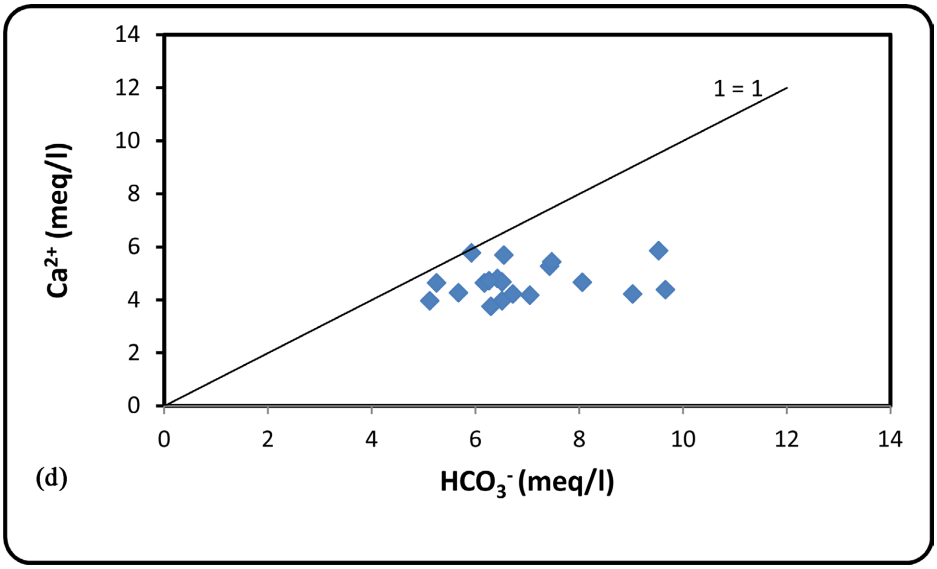

Figure 8. Diagrams of (a) $Ca^{2+} + Mg^{2+}$ versus $HCO_3^- + SO_4^{2-}$; (b) $(Ca^{2+} + Mg^{2+})$ - $(HCO_3^- - SO_4^{2-})$ versus Na^+ - Cl^-; (c) total cation versus $Ca^{2+} + Mg^{2+}$; and (d) Ca^{2+} versus HCO_3^-.

supported by the computed molar ratio of Ca/Mg (**Table 4**) and plot of total cation versus $Ca^{2+} + Mg^{2+}$ (**Figure 8(c)**).

The computed molar ratios of Ca/Mg ranged from 1.61 - 15.21 with a mean 4.49. With the exception of samples HAGW 2 and HAGW 5 from gravely sand aquifer, in all the remaining samples the molar ratios of Ca/Mg are greater than 2. According to Tahoora *et al.* [37], a molar ratio Ca/Mg greater than 2 indicates silicate weathering process a major process that control the presence of Ca and Mg ions in the groundwater chemistry. The plot total cation versus $Ca^{2+} + Mg^{2+}$, where all the groundwater samples fall above the 1:1 equline, indicating the dominancy of silicate weathering and the significant contribution of sodium to the total cations (**Figure 8(c)**) [29]. It also shows the removal of Ca and Mg ions from the groundwater due to the normal ion exchange process.

The $HCO_3^- / HCO_3^- + SO_4^{2-}$ ratio is used to determine the role of carbonation and sulphide oxidation geochemical processes in the chemistry of the groundwater [22]. According to Babita *et al.* [22], if the ratio is equivalent to one, it indicates carbonic acid weathering (dissolution and hydrolysis), exhausting protons from atmospheric CO_2 (Equation (5)), ratio of 0.5 implies the role of both sulphide oxidation and carbonic weathering processes, ratio less than 0.5 signify sulphide oxidation. In the present case, the ratios vary between 0.6 and 1 (**Table 4**). High bicarbonate concentrations and the ratios of $HCO_3^- / HCO_3^- + SO_4^{2-}$ between 0.6 to 1 in all the groundwater samples suggest that carbonate acid weathering (dissolution and hydrolysis) control the solute acquisition process in the groundwater chemistry of the study area. However, the role of pure dissolution process in the chemistry of the groundwater in the area is not significant as shown in the Fig 8A. Hydrolysis is the main process that controls groundwater chemistry in the study area. As shown in the plot of Ca ion versus HCO_3^-,

(**Figure 8(d)**), all the samples are lying below the equiline, indicating the existence of more HCO_3^- concentration over Ca ion. Even though, there is also a release of Ca ion from calcite, gypsum and plagioclase (Equations (7)-(9)), its existence having low concentrations with respect to HCO_3^- ion that have the same sources (Equations (7) and (8)) with it might be due to normal ion exchange process that consumed Ca and Mg ions from groundwater. This process can be ascribed to the exchange of calcium and magnesium in groundwater by sodium and potassium in the shale beds of the host formation.

Therefore, in the study area the groundwater chemistry is primarily controlled by weathering of the rock-forming minerals that constitute the Paleozoic-Mesozoic sedimentary successions. Since, the aquifer is shallow, the dissolution of carbon dioxide, derived from the decay of organic matter and/or atmosphere is the main source for hydrogen ion, H^+ (Equation (6)), generating reactions which in turn facilitating chemical weathering of gypsum, silicates, aluminosilicates and carbonate minerals.

$$CO_2 + H_2O \leftrightarrow H_2CO_3 \tag{5}$$

$$H_2CO_3 \leftrightarrow H^+ + HCO_3^- \tag{6}$$

The hydrogen ion produced in the dissociation of carbonic acid (Equation (6)) results in the decrease in pH and an increase in bicarbonate concentration in groundwater. Acidic to neutral pH (6.55 to 7.26) of the groundwater indicate that H^+ produced from dissociation of carbonic acid reacted further with silicates (Equations (8) and (10)), gypsum (Equation (9)) and calcite (Equation (7)) to neutralize the acidity produced and liberate associated anions (HCO_3^- and SO_4^{2-}) and cations (Na^+, Ca^{2+}, Mg^{2+} and K^+). Hydrolysis of pyroxene, K-feldspar, Na-feldspar and biotite, is also a possible source for HCO_3^-, Na^+, Ca^{2+}, Mg^{2+} and K^+ ions. Groundwater is characteristically saturated to be oversaturated with respect to calcite. For SO_4^{2-} to occur as the dominant anion, only very small amounts of gypsum need to be dissolved. Since gypsum are found occurring as a fine grained minerals in the petrographic analyses of limestone, as water moves along its flow paths and enters the gypsum zone, dissolution of gypsum (Equation (9)) causes the water to become rich with Ca^{2+} and SO_4^{2-} as the dominant ions. Because of the common-ion effect, the additional Ca^{2+} often produces water that is saturated with respect to calcite. Lower SO_4^{2-} values in most of the samples suggest rare occurrence of gypsum layer in the limestone unit.

The intercalated shale beds are also the sources of sodium and chloride ions. When the water enters the shale beds, it incorporates sodium and chloride ions, which are found in major and minor amounts, respectively, in groundwater. Waters draining shale often contain chloride and sodium. These are thought to originate from seawater trapped in the shale at the time of deposition, but the form in which these ions are stored in shale is not known [38]. Significant difference in the concentration of sodium and chloride ions in groundwater suggests the existence of additional source for Na^+ ion besides to the shale beds and normal ion exchange process. This is due to hydrolysis of feldspar (Equation (10)) that occurs as miner-

als having angular to sub-angular grained nature in the limestone.

$$CaCO_3 + CO_2 + H_2O \leftrightarrow Ca^{2+} + 2HCO_3^- \quad (7)$$

$$CaAl_2Si_2O_8\left(\text{anorthite}\right) + 2CO_2 + 3H_2O \rightarrow Al_2Si_2O_5\left(OH\right)_4 + Ca^{2+} + 2HCO_3^- \quad (8)$$

$$CaSO_4 \cdot 2H_2O \rightarrow Ca^{2+} + SO_4^{2-} + 2H_2O \quad (9)$$

$$2NaAlSi_3O_8 + 2\left(H^+ + HCO_3^-\right) + H_2O \rightarrow Al_2Si_2O_5\left(OH\right)_4 + 2Na^+ + 2HCO_3^- + 4SiO_2 \quad (10)$$

5. Conclusions

Unconfined and confined aquifers were identified in the sub basin underlain by Paleozoic-Mesozoic sedimentary successions. Groundwater chemistry is strongly controlled by the mineralogical composition of the underlying rocks. The groundwater is acidic to neutral, fresh, and hard to very hard. Ca^{2+}, Na^+, HCO_3^- and SO_4^{2-} are the dominant ions in relation to Mg^{2+}, K^+, and Cl^- ions. The dominant hydrochemical facies are Ca-Na-HCO_3 (40%), Ca-HCO_3 (20%), Ca-Mg-Na-HCO_3 (10%) and Ca-Na-HCO_3-SO_4 (10%).

The main chemical characteristics of the groundwater from these aquifers can be accounted for by a combination of the following geochemical processes that are interrelated: dissociation of carbonic acid to produce pH values in the range 6.5 - 7.26 and HCO_3^- values in the range 300 - 600 mg/l, dissolution of calcite to produce Ca^{2+} and HCO_3^- ions, dissolution of gypsum ($CaSO_4 \cdot 2H_2O$) to produce SO_4^{2-} and Ca^{2+} ions, hydrolysis of silicate and aluminosilicate minerals to produce sodium, magnesium, potassium and bicarbonate ions, normal ion exchange process to deplete calcium and magnesium ions from the water and produce sodium and potassium ions, and incorporation of sodium and chloride ions from shale beds.

This study was conducted using the groundwater from hand dug wells which can be used as a basis for more characterization of hydrochemical facies of the study area. More insights on the impact of deeper aquifers on the chemistry of the groundwater may be derived from analyses of the groundwater from deep wells that are found in the area.

Acknowledgments

The primary data collection was sponsored by the Nile Basin Initiatives (NBI/ATP). NBI is duly acknowledged for this.

Conflicts of Interest

The authors declare no conflicts of interest regarding the publication of this paper.

References

[1] Sefie, A., Aris, A.Z., Shamsuddin, M.K.N., *et al.* (2015) Hydrogeochemistry of

Groundwater from Different Aquifer in Lower Kelantan Basin, Kelantan, Malaysia. *Procedia Environmental Sciences*, **30**, 151-156. https://doi.org/10.1016/j.proenv.2015.10.027

[2] United Nations Environment Program (UNEP) (1999) Global Environment Outlook 2000. Earthscan, London.

[3] Tadesse, N. (2006) Surface Waters Potential of the Hantebet Basin, Tigray, Northern Ethiopia. *Agricultural Engineering International*, **8**, 1-31.

[4] Tadesse, N., Bairu, A., Bheemalingeswara, K. and Gyohannes, T. (2011) Suitability of Groundwater Quality for Irrigation with Reference to Hand Dug Wells, Hantebet Catchment, Tigray, Northern Ethiopia. *Momona Ethiopian Journal of Science*, **3**, 31-47. https://doi.org/10.4314/mejs.v3i2.67711

[5] Nyssen, J., Poesen, J., Descheemaeker, K., Haregeweyn, N., Haile, M., Moeyersons, J., Frankl, A., Govers, G., Munro, N. and Deckers, J. (2008) Effects of Region-Wide Soil and Water Conservation in Semi-Arid Areas: The Case of Northern Ethiopia. *Journal of Geomorphology*, **52**, 291-315. https://doi.org/10.1127/0372-8854/2008/0052-0291

[6] Alemu, T., Abdelsalam, M.G., Dawit, E.L., Atnafu, B. and Mickus, K.L. (2018) The Paleozoic Mesozoic Mekele Sedimentary Basin in Ethiopia: An Example of an Exhumed Intracontinental Sag (ICONS) Basin. *Journal of African Earth Sciences*, **143**, 40-58. https://doi.org/10.1016/j.jafrearsci.2018.03.010

[7] Sembroni, A., Molin, P., Dramis, F. and Abebe, B. (2017) Geology of the Tekeze River Basin (Northern Ethiopia). *Journal of Maps*, **13**, 621-631. https://doi.org/10.1080/17445647.2017.1351907

[8] Abbate, E., Azzaroli, A., Zanettin, B. and Visentin, E.J. (1968) A Geologic and Petrographic Mission of the "Consiglio Nazionaledelle Ricerche" to Ethiopia, 1967-1968: Preliminary Results. *Bollettino Società Geologica Italiana*, **87**, 561-580.

[9] Arkin, Y., Beyth, M., Dow, D.B., Levitte, D., Haile, T. and Hailu, T. (1971) Geological Map of Mekele Sheet Area ND 3711, Tigre Province. Geological Survey of Ethiopia, Addis Ababa.

[10] Beyth, M. (1972) Paleozoic-Mesozoic Sedimentary Basins of Mekele Outlier, Northern Ethiopia. *Association of American Petroleum Geologists Bulletin*, **56**, 2426-2439. https://doi.org/10.1306/819A422A-16C5-11D7-8645000102C1865D

[11] Bosellini, A., Russo, A., Fantozzi, P.L., Assefa, G. and Tadesse, S. (1997) The Mesozoic Succession of the Mekele Outlier (Tigre Province, Ethiopia). *Memorie Scienze Geologiche*, **49**, 95-116.

[12] Dow, D.B., Beyth, M. and Hailu, T. (1971) Paleozoic Glacial Rocks Recently Discovered in Northern Ethiopia. *Geological Magazine*, **108**, 53-59. https://doi.org/10.1017/S0016756800050962

[13] Ethiopian Institute of Geological Survey (EIGS) (1993) Hydrogeological Map of Ethiopia, 1:2,000,000 Scale. Ministry of Mines and Energy and Ethiopian Institute of Geological Survey (EIGS), Addis Ababa.

[14] Ethiopian Institute of Geological Survey (EIGS) (1996) Explanation of the Geological Map of Ethiopia (Scale 1:2,000,000). 2nd Edition, Ethiopian Institute of Geological Survey, Addis Ababa, 79.

[15] Enkurie, D.L. (2010) Adigrat Sandstone in Northern and Central Ethiopia: Stratigraphy, Facies, Depositional Environments and Palynology. PhD Thesis, University of Berlin, Berlin, 162.

[16] Levitte, D. (1970) On the Geology of the Central Part of the Mekele Sheet,

1:250,000: Ethiopian Geological Survey.

[17] Getaneh, W. (2016) Sulfides, Stable Isotopes and Other Diagenetic Features of the Mesozoic Carbonate-Marl-Shale Succession in Northern Ethiopia. *SINET*: *Ethiopian Journal of Science*, **39**, 34-49.

[18] Ermias, G., Tenalem, A., Seifu, K., Mulugeta, A., Stefan, W. and Frank, W. (2015) Conceptual Groundwater Flow Model of the Mekelle Paleozoic-Mesozoic Sedimentary Outlier and Surroundings (Northern Ethiopia) Using Environmental Isotopes and Dissolved Ions. *Hydrogeology Journal*, **23**, 649-672. https://doi.org/10.1007/s10040-015-1243-4

[19] Tewodros, A., Albrecht, L. and Martin, D. (2020) Environmental Isotope and Hydrochemical Characteristics of Groundwater in Central Portion of Mekelle Sedimentary Outlier, Northern Ethiopia. *Journal of African Earth Sciences*, **171**, Article ID: 103953. https://doi.org/10.1016/j.jafrearsci.2020.103953

[20] Chernet, T. (1993) Hydrogeology of Ethiopia and Water Resources Development. EIGS, Addis Ababa.

[21] Nata, T., Miruts, H. and Bheemalingeswara, K. (2009) Hydrogeological Investigation: A Case Study on the Groundwater Potential Assessment in the Hantebet Catchment, Tigray, Northern Ethiopia. *International Journal of Tropical Drylands*, **2**, 55-65.

[22] Neogi, B., Singh, A.K., Pathak, D.D. and Chaturvedi, A. (2017) Hydrogeochemistry of Coal Mine Water of North Karanpura Coalfields, India: Implication for Solute Acquisition Processes, Dissolved Fluxes and Water Quality Assessment. *Environmental Earth Sciences,* **76**, Article No: 489. https://doi.org/10.1007/s12665-017-6813-4

[23] Sang, Y.C., Rajendran, R., Venkatramanan, S., Sekar, S., Ranganathan, P.C., Oh, Y.Y. and Elzain, H.E. (2020) Processes and Characteristics of Hydrogeochemical Variations between Unconfined and Confined Aquifer Systems: A Case Study of the Nakdong River Basin in Busan City, Korea. *Environmental Science and Pollution Research International*, **27**, 10087-10102. https://doi.org/10.1007/s11356-019-07451-6

[24] Schoeller, H. (1967) Qualitative Evaluation of Groundwater Resources. In: Schoeller, H., Ed., *Methods and Techniques of Groundwater Investigation and Development*; *Water Resource Series No.* 33, UNESCO, Paris, 44-52.

[25] Faisal, K.Z., Saad, M., Manoj, M. and Elkhedr, I. (2016) Evaluation of Groundwater Chemistry and Its Impact on Drinking and Irrigation Water Quality in the Eastern Part of the Central Arabian Graben and Trough System, Saudi Arabia. *Journal of African Earth Sciences*, **120**, 208-219. https://doi.org/10.1016/j.jafrearsci.2016.05.012

[26] Soltan, M.E. (1999) Evaluation of Groundwater Quality in Dakhla Oasis (Egyptian Western Desert). *Environmental Monitoring and Assessment*, **57**, 157-168. https://doi.org/10.1023/A:1005948930316

[27] International Institute for Environment and Development (IIED) (2002) Breaking New Ground. Final Report of the Mining, Minerals and Sustainable Development Project. International Institute for Environment and Development, Earthscan Publications Ltd., London.

[28] Sakram, G. and Adimalla, N. (2018) Hydrogeochemical Characterization and Assessment of Water Suitability for Drinking and Irrigation in Crystalline Rocks of Mothkur Region, Telangana State, South India. *Applied Water Science*, **8**, 143. https://doi.org/10.1007/s13201-018-0787-6

[29] Sajil Kumar, P.J. and James, E.J. (2016) Identification of Hydrogeochemical Processes in the Coimbatore District, Tamil Nadu, India. *Hydrological Sciences Journal*, **61**, 719-731. https://doi.org/10.1080/02626667.2015.1022551

[30] Meybeck, M. (1987) Global Chemical Weathering of Surficial Rocks Estimated from River Dissolved Loads. *American Journal of Science*, **287**, 401-428. https://doi.org/10.2475/ajs.287.5.401

[31] Deutsch, W.J. (1997) Groundwater Geochemistry: Fundamentals and Applications to Contamination. CRC Press, New York, 232.

[32] Elango, L. and Kannan, R. (2007) Chapter 11 Rock-Water Interaction and Its Control on Chemical Composition of Groundwater. *Developments in Environmental Science*, **5**, 229-243. https://doi.org/10.1016/S1474-8177(07)05011-5

[33] Adomako, D., Osae, S., Akiti, T.T., Faye, S. and Maloszewski, P. (2011) Geochemical and Isotopic Studies of Groundwater Conditions in the Densu River Basin of Ghana. *Environmental Earth Sciences*, **62**, 1071-1084. https://doi.org/10.1007/s12665-010-0595-2

[34] Fisher, R. and Mullican, F.W. (1997) Hydrochemical Evolution of Sodium-Sulfate and Sodium-Chloride Groundwater beneath the Northern Chihuahuan Desert, Trans-Pecos, Texas, USA. *Hydrogeology Journal*, **5**, 4-16. https://doi.org/10.1007/s100400050102

[35] Rajmohan, N. and Elango, L. (2004) Identification and Evolution of Hydrogeochemical Processes in the Groundwater Environment in an Area of the Palar and Cheyyar River Basins, Southern India. *Environmental Geology*, **46**, 47-61.

[36] Rambabu Singh, Syed, T.H., Kumar, S., Kumar, M. and Venkatesh, A.S. (2017) Hydrogeochemical Assessment of Surface and Groundwater Resources of Korba Coalfield, Central India: Environmental Implications. *Arabian Journal of Geosciences*, **10**, Article No. 318. https://doi.org/10.1007/s12517-017-3098-6

[37] Tahoora, S.N., Mohammad, F.R., Ahmad, Z.A., Wan Nor, A.S., Hafizan, J. and Kazem, F. (2014) Identification of the Hydrogeochemical Processes in Groundwater Using Classic Integrated Geochemical Methods and Geostatistical Techniques, in Amol-Babol Plain, Iran. *The Scientific World Journal*, **2014**, Article ID: 419058. https://doi.org/10.1155/2014/419058

[38] Drever, J.I. (1997) The Geochemistry of Natural Waters: Surface and Groundwater Environments. 3rd Edition, Prentice Hall, Hoboken, 436.